

Freshening of Subsurface Waters in the Northwest Pacific Subtropical Gyre: Observations and Dynamics

YOUFANG YAN

State Key Laboratory of Tropical Oceanography, and South China Sea Institute of Oceanology, Chinese Academy of Sciences, Guangzhou, China

ERIC P. CHASSIGNET

Center for Ocean–Atmospheric Prediction Studies, and Department of Earth, Ocean and Atmospheric Science, The Florida State University, Tallahassee, Florida

YIQUAN QI

State Key Laboratory of Tropical Oceanography, and South China Sea Institute of Oceanology, Chinese Academy of Sciences, Guangzhou, China

WILLIAM K. DEWAR

Department of Earth, Ocean and Atmospheric Science, The Florida State University, Tallahassee, Florida

(Manuscript received 3 January 2013, in final form 17 July 2013)

ABSTRACT

Subsurface salinity anomalies propagating between mid- and low latitudes along isopycnal surfaces have been shown to play an important role in modulating ocean and climate variability. In this study, a sustained freshening and southwestward propagation of subsurface salinity anomalies in the northwest Pacific subtropical gyre and its dynamical mechanism are investigated using observations, numerical outputs, and a predictive model. Analyses of the observations show a pronounced subsurface freshening with salinity decreasing about 0.25 PSU near the $24.5\text{-}\sigma_\theta$ surface in the northwest Pacific subtropical gyre during 2003–11. This freshening is found to be related to the surface forcing of salinity anomalies in the outcrop zone ($25^\circ\text{--}35^\circ\text{N}$, $130^\circ\text{--}160^\circ\text{E}$). A predictive model based on the assumption of salinity conservation along the outcrop isopycnals is derived and used to examine this surface-forcing mechanism. The resemblance between the spatial structures of the subsurface salinity derived from the predictive model and from observations and numerical outputs suggests that subsurface salinity anomalies are ventilated over the outcrop zone. A salinity anomaly with an amplitude of about 0.25 PSU generated by the surface forcing is subducted in the outcrop zone and then propagates southwestward, accompanied by potential vorticity anomalies, to the east of Luzon Strait ($\sim 15^\circ\text{N}$) in roughly one year. When the anomalies reach 15°N , they turn and move gradually eastward toward the central Pacific, associated with an eastward countercurrent on the southern subtropical gyre.

1. Introduction

Because of the large thermal inertia of the ocean, changes in water mass properties on interannual to decadal scales have attracted considerable attention in

studies of ocean and climate variability (Bindoff and Church 1992; Deser et al. 1996; Gu and Philander 1997; Johnson and Orsi 1997; Bryden et al. 2003; Tomczak and Liefvink 2005; Kilpatrick et al. 2011). Water mass properties can be characterized either by temperature and salinity or by density. Potential density σ_θ referenced to the ocean surface pressure can be expressed as a combination of potential temperature θ and salinity S , that is, $d\sigma_\theta = -\alpha d\theta + \beta dS$, where α and β are the thermal expansion and haline contraction coefficient, respectively. Water masses move along neutral surfaces

Corresponding author address: Youfang Yan, State Key Laboratory of Tropical Oceanography, and South China Sea Institute of Oceanology, Chinese Academy of Sciences, 164 West Xingang Road, Guangzhou, 510301, China.
E-mail: youfangyan@scsio.ac.cn

(McDougall 1987), which we will here approximate using σ_θ -isopycnal surfaces. On σ_θ surfaces, salinity has proven to be a useful tracer of water mass motions in the past studies (Parr 1938; Montgomery 1938). Furthermore, advection of salinity anomalies from the mid- to low latitudes along isopycnal surfaces could also couple the subtropical and tropical oceans, modify the subsurface temperature [$d\theta|_\sigma = (\beta/\alpha)dS|_\sigma$], and consequently affect tropical climate changes (Lukas 2001; Schneider 2004; Maes et al. 2005; Williams et al. 2007; Balaguru et al. 2012). Thus, salinity is not only a dynamical tracer conservatively following parcels' trajectory along isopycnal surfaces but also exhibits an important thermodynamic effect on climate variability.

Important technological advances for the past decades enabled impressive progress in the description and understanding of the subsurface salinity variability. Argo-profiling floats arrays, in synergy with in situ hydrographic observations and high-resolution ocean models, revealed an important role of the late-winter surface forcing in the subsurface salinity variability, with salinity anomalies preferentially formed in the central and eastern subtropical Pacific outcrop region and propagating southwestward to the western Pacific (Lukas 2001; Yeager and Large 2004; Nonaka and Sasaki 2007; Ren and Riser 2010; Sasaki et al. 2010). For example, using Argo and World Ocean Circulation Experiment (WOCE) observations, Ren and Riser (2010) showed that subsurface decadal time-scale salinity anomalies are subducted in the eastern subtropical North Pacific and propagate southwestward to the western Pacific along geostrophic streamlines. A similar time-scale propagation of salinity anomalies along contours of mean potential vorticity was found by Nonaka and Sasaki (2007) and Sasaki et al. (2010). Using a fully coupled ocean-atmosphere general circulation model, Pierce et al. (2000) showed clearly that salinity anomalies are able to propagate from the eastern subtropical subduction regions to the equator along isopycnal surfaces on time scales of ~ 7 yr, although this signal became difficult to trace as a coherent entity in the equatorial region. However, this result is quite different from those of Kessler (1999) and Suga et al. (2000), who found no direct linkage between the salinity variability on isopycnal surfaces and upstream changes at winter density outcrops in the Pacific Ocean based on hydrographic section observations. Using a model forced with the most realistic surface products available over the 40 years, Yeager and Large (2004) suggested that the largest interannual anomalies of spiciness (compensating potential temperature and salinity variation on an isopycnal) near the 25.5-isopycnal surface in the Pacific are generated by diapycnal mixing at the base of the mixed layer in the

eastern subtropics. This diapycnal-mixing mechanism, driven by large unstable salinity gradients in conjunction with weak stratification occurring in the eastern subtropics of the South Pacific, was confirmed by Luo et al. (2005). In addition, Luo et al. (2005) also showed that spiciness anomalies can be created along isopycnals that outcrop to the surface through the subduction processes. On the basis of theoretical analysis and numerical model output, Nonaka and Sasaki (2007) suggested that cool surface temperature anomalies could generate meridional migrations of density outcrop lines and induce warm and salty subducted anomalies on isopycnal surfaces. Subducted warm and salty anomalies propagate to the equatorial region in roughly 5 years and influence the isopycnal temperature and salinity anomalies in the equatorial region.

Although there has been some success in linking the subsurface salinity variability to the surface anomaly, a controversy about its generation mechanism still exists. In addition, the downstream impact of subducted subtropical anomalies on the variability of low-latitude region especially in the western tropical Pacific has not been well understood. In the western Pacific, advection of the central and eastern subtropical Pacific outcrop anomalies is primarily through the North Equatorial Current (NEC). The anomalies carried by the NEC can flow back either to the subtropics via the Kuroshio or to the tropics via the Mindanao Current (MC; Fig. 1). According to Schneider (2000), spiciness anomalies in the western tropical Pacific are generated by wind-driven anomalous advection across temperature and salinity fronts and transported subsequently to the equator via the MC. On the basis of Argo observations, Li et al. (2012) suggested that subsurface spiciness variability in the western tropical Pacific is generated locally by anomalous cross-front geostrophic advection, which is closely related to ENSO. Using observations and assimilation products, Yan et al. (2012) examined the interannual variability of subsurface salinity in the east of Luzon Strait and found a freshening trend occurring at ~ 200 m. This freshening involves neither the upstream changes in the eastern North Pacific nor the local surface freshwater flux and geostrophic flow anomaly in the northwest Pacific. However, it remains unclear what causes the subsurface salinity anomalies in the east of Luzon Strait. Are they related to the remote surface salinity anomalies in the northwest Pacific through the subduction processes? These questions lead us further to examine the subsurface salinity variability with a main focus on its generation and propagation mechanisms in the Northwest Pacific based on observations, numerical outputs, and a predictive model.

The rest of the paper is organized as follows. Section 2 briefly describes the datasets used in this study. Section 3

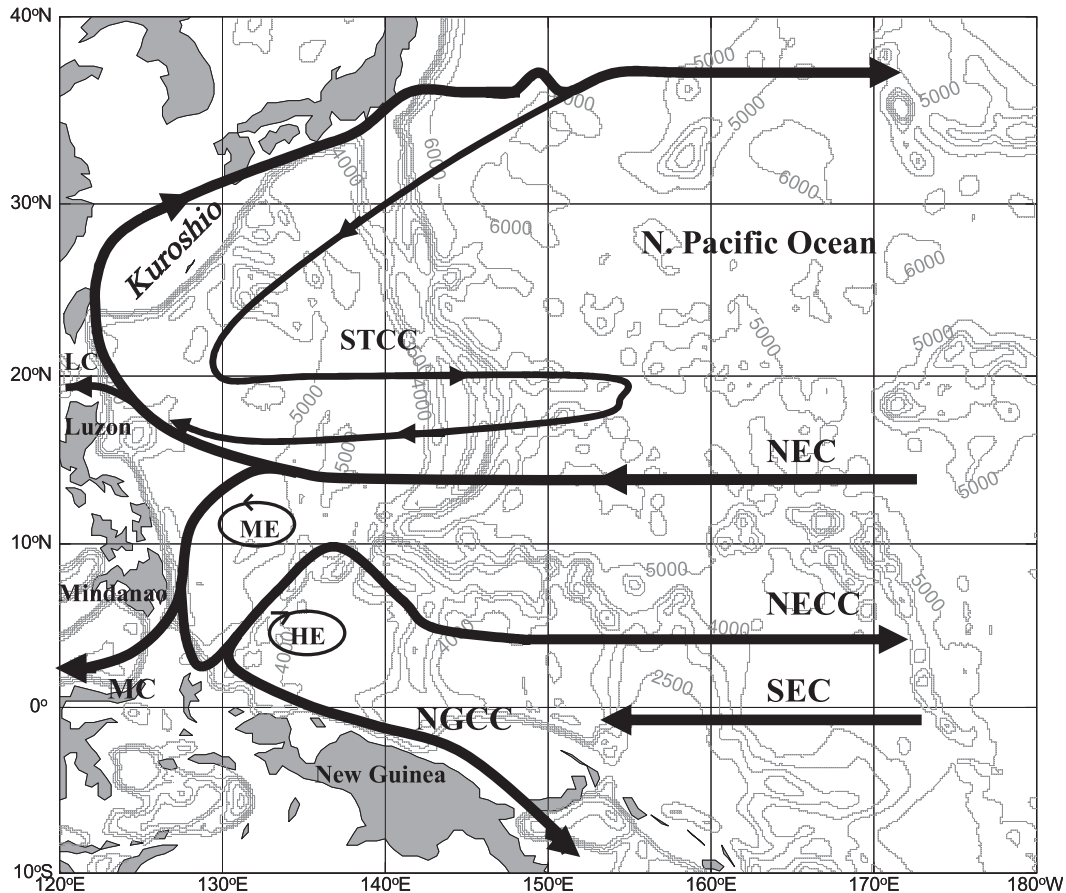


FIG. 1. Schematic chart of the major large-scale circulation in the western Pacific superimposed upon a map of bottom topography denoted by gray contours. Acronyms denote the Luzon Current (LC), Subtropical Counter-current (STCC), the MC, NEC, the North Equatorial Countercurrent (NECC), the South Equatorial Current (SEC), the New Guinea Coastal Current (NGCC), and the Mindanao (ME) and Halmahera eddies (HE).

presents the observed and modeled subsurface salinity variations and their propagation. The generation mechanism of these anomalies is examined in section 4, followed by a summary and discussion of the main results in section 5.

2. Datasets

To study the subsurface salinity variability, we utilize the monthly temperature and salinity dataset compiled by Hosoda et al. (2008) that combines quality-controlled Argo-profiling data, Triangle Trans-Ocean Buoy Network buoy measurements and other available conductivity–temperature–depth (CTD) observations. This dataset is known as the Monthly Objective Analysis using the Argo data (MOAA) Grid Point Value (GPV) and has a $1^\circ \times 1^\circ$ spatial resolution for the 2000-m upper ocean. Details of data processing, gridding, and error estimation of the MOAA-GPV are described in Hosoda et al. (2008). The

MOAA-GPV has been widely used to explore the interannual to decadal variability in the northwest Pacific subtropical gyre (Tomita et al. 2010; Li et al. 2012; Qiu and Chen 2012). As the MOAA-GPV dataset became available in 2001 following the start of the international Argo project, the focus of our following analyses is on the recent change in salinity between January 2003 and December 2011. The salinity anomaly in each month is defined as the deviation of salinity mean over the period of 2003–11 for each pressure layer, with respect to the discrepancy of the climatological-mean distribution of salinity between the *World Ocean Atlas 2009* data (hereafter *WOA09*; Antonov et al. 2010; Locarnini et al. 2010) and MOAA-GPV dataset, as shown in Fig. 2.

To further examine the mechanisms potentially responsible for salinity variability, we also use the assimilation products of the Estimating the Circulation & Climate of the Ocean (ECCO) project provided by the Jet Propulsion

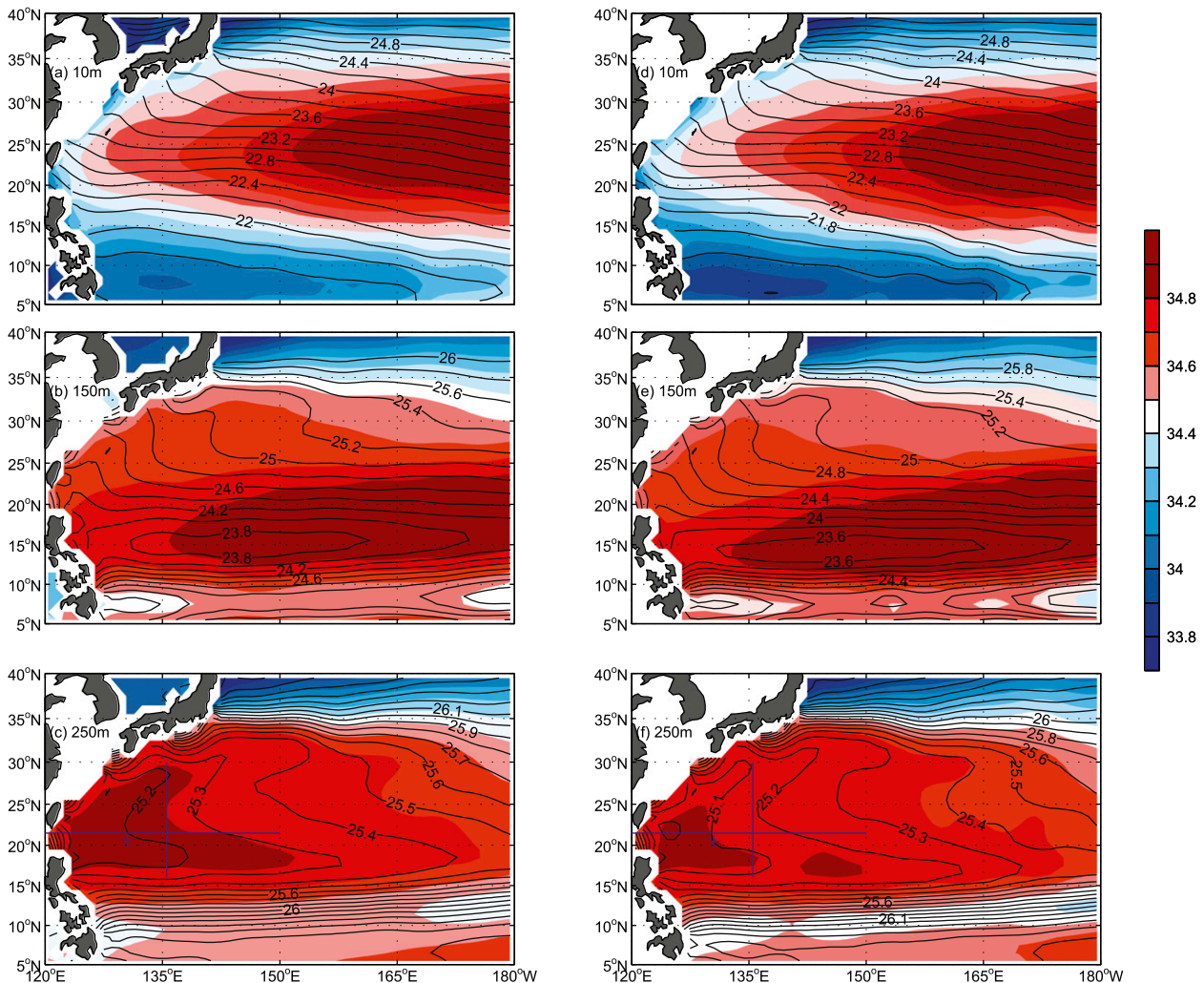


FIG. 2. Climatological distributions of annual-mean salinity (color shades) and potential density (contours) at depths (a) 10, (b) 150, and (c) 250 m from the temperature and salinity of the WOA09; (d)–(f) as in (a)–(c), but for the annual-mean salinity of the MOAA-GPV data during the period 2003–11. The grid point (20.5°N, 130.5°E) and the sections along 21.5°N and 135.5°E used for calculating the salinity and its anomaly in Figs. 4–6 are shown by a blue plus sign and intersecting blue lines, respectively.

Laboratory (JPL; <http://ecco.jpl.nasa.gov>). The ECCO model is a near-global version of the Massachusetts Institute of Technology (MIT) Ocean General Circulation Model (Marshall et al. 1997). It assimilates altimetric sea level anomalies [Ocean Topography Experiment (TOPEX)/Poseidon and *JASON-1*], in situ temperature profiles [XBT, Argo, and Tropical Atmosphere Ocean (TAO)], Levitus climatological temperature and salinity, and the National Centers for Environmental Prediction (NCEP) surface fluxes using a Kalman filter. The model coverage is nearly global (79.5°S–78.5°N) with a telescoping meridional grid at a $1/3^\circ$ resolution in the tropics (20°S–20°N), and gradually increasing to 1° resolution away from the tropics. The resolution in longitude is 1° . There are 46 vertical levels with 10 m spacing for the

150 m upper ocean, then gradually increasing to 400 m spacing at its maximum depth. The model is forced by NCEP reanalysis products (12-hourly wind stress, daily sea heat, and freshwater fluxes) and time means are replaced by those of the Comprehensive Ocean–Atmosphere Data Set. Model fields are available as 10-day averages. Additional descriptions of the model and detailed comparisons of the model outputs with the various observational data, including temperature, salinity, and velocity in the tropical Pacific and Indian Oceans, are provided by Lee et al. (2002). The ECCO-JPL products have been extensively applied to analyze the mixed layer temperature and salinity budget in the tropical and subtropical Pacific Ocean (Kim et al. 2004; Halkides and Lee 2009; van der Werf et al. 2009; Yan et al. 2012).

3. Vertical structure of the salinity change in the northwest Pacific

Before examining the vertical structure of the interannual salinity change, it is necessary to know the long-term-mean distribution of salinity, density, and mixed layer depth (MLD) in the northwest Pacific. Figure 2 shows the distributions of annual-mean salinity as well as the potential density for *WOA09* and MOAA-GPV at 10, 150, and 250 m in the northwest Pacific, approximately representing the surface, the base of mixed layer, and the permanent thermocline, respectively. At the surface, the salinity distribution broadly reflects the pattern of evaporation minus precipitation (Peixoto and Oort 1992; Talley 2002). A general feature of this surface distribution is near-equatorial (south of 15°N) and higher-latitude (north of 35°N) local minima and subtropical (15°–35°N) maxima. The difference between the near-equatorial minimum and the subtropical maxima is roughly 1.0 PSU (Fig. 2a). The isopycnal lines at this surface are nearly zonal except for a slight tilt near the equatorial region, with the highest value in the high latitudes and the lowest in the warm waters of the tropics. At a depth of 150 m, the difference in salinity between the near-equatorial and the subtropical region is less distinct than that of the surface. At this depth, salinity increases from a low of 33.8 to 34.6 PSU at the near-equatorial region. On the other hand, the high-salt tongue in the subtropical region extends farther southwestward along 18°N to the western boundary (Fig. 2b). At a depth of 250 m, the salinity pattern is much the same as that at 150 m near the equator and in the high latitudes, but there is a new feature in the subtropical regions (Fig. 2c). The high values of salinity are found in the western part of the subtropical gyres, with its maximum located in the northwest Pacific subtropical gyre near the Luzon Strait. The pattern of potential density at 250 m differs from that of the surface in having a southwestward and then eastward extension of lower density and higher salinity at the western boundary.

The general distributions of salinity and potential density for the MOAA-GPV are similar to those of *WOA09*, but some discrepancies are also found (Figs. 2d–f). For example, the position of the 22.0-isopycnal line differs between *WOA09* and MOAA-GPV at the surface (Figs. 2a,d). Large differences in salinity and potential density between *WOA09* and MOAA-GPV are also found at 150- and 250-m levels (Figs. 2b–f). The area of high-salinity water (≥ 34.8 PSU) at the depth of 250 m in the western part of the subtropical gyre for *WOA09* becomes smaller for MOAA-GPV, and the potential density at this level tends to be smaller in MOAA-GPV. The reason for the discrepancy between the *WOA09* and

MOAA-GPV is not clear. One possible explanation is that the averaging times of these two datasets are different. For instance, the temperature and salinity climatologies for the *WOA09* are the average of five decadal climatologies for the periods 1955–64, 1965–74, 1975–84, 1985–94, and 1995–2006 (Antonov et al. 2010; Locarnini et al. 2010), while the temperature and salinity averages for MOAA-GPV are for the period 2003–11. Another possible explanation is that there has been a continued freshening of subsurface water during the last decade (2003–11), and thus we see the salinity decrease in the western part of the subtropical gyre. In other words, the averages of temperature and salinity for MOAA-GPV are more representative of the ocean mean state in the last decade.

The climatological distribution of MLD and potential density σ_θ at the base of the MLD in winter (December–February) and summer (July–September) are shown in Fig. 3 for *WOA09* and MOAA-GPV. Note that MLD here is defined as the depth at which σ_θ differs by 0.125 kg m^{-3} from the surface. As shown in Fig. 3c, the depth of summer mixed layer is shallow, approximately 20–40 m over most of the northwest Pacific. The corresponding density at the base of the MLD is about 21.0–24.0 kg m^{-3} . Compared to the summer MLDs, winter MLDs are significantly deeper, ranging from 60 to 140 m. The shallower winter MLDs, about 60 m, are located along the southern rim of the North Pacific subtropical basin, and there has a tendency toward larger value of MLDs at higher latitudes (Fig. 3a). The maximum MLD of about 140 m occurs along the Kuroshio Extension from the coast of Japan to $\sim 160^\circ\text{E}$ and is closely related to the strong air–sea exchange and strong subduction in the western North Pacific (Qiu and Huang 1995; Chen et al. 2010; Liu and Huang 2012). This result is consistent with that of Qiu and Huang (1995) and Deser et al. (1996). In addition, this result also resembles that of the MOAA-GPV (Figs. 3e–g), although some differences are found.

The vertical structures of salinity and its anomalies in the northwest Pacific subtropical gyre are first examined using time–pressure plots from the MOAA-GPV dataset at a typical site (20.5°N, 130.5°E), located at the center of the freshening region (Li et al. 2012; Yan et al. 2012). As stated earlier, the salinity anomaly for each month and each layer is defined as the deviation of monthly salinity mean over the period 2003–11. The salinity field (Fig. 4a) exhibits a pronounced variability between the σ_θ surfaces of 23.5–25.2 with salinity decreasing from 35.0 to 34.8 PSU during the period 2003–11. The anomalous salinity field (Fig. 4b) shows a series of anomalous pulses beginning in 2003 that appear to originate at the base of the mixed layer during the cold season and then penetrate downward into the oceanic interior. These

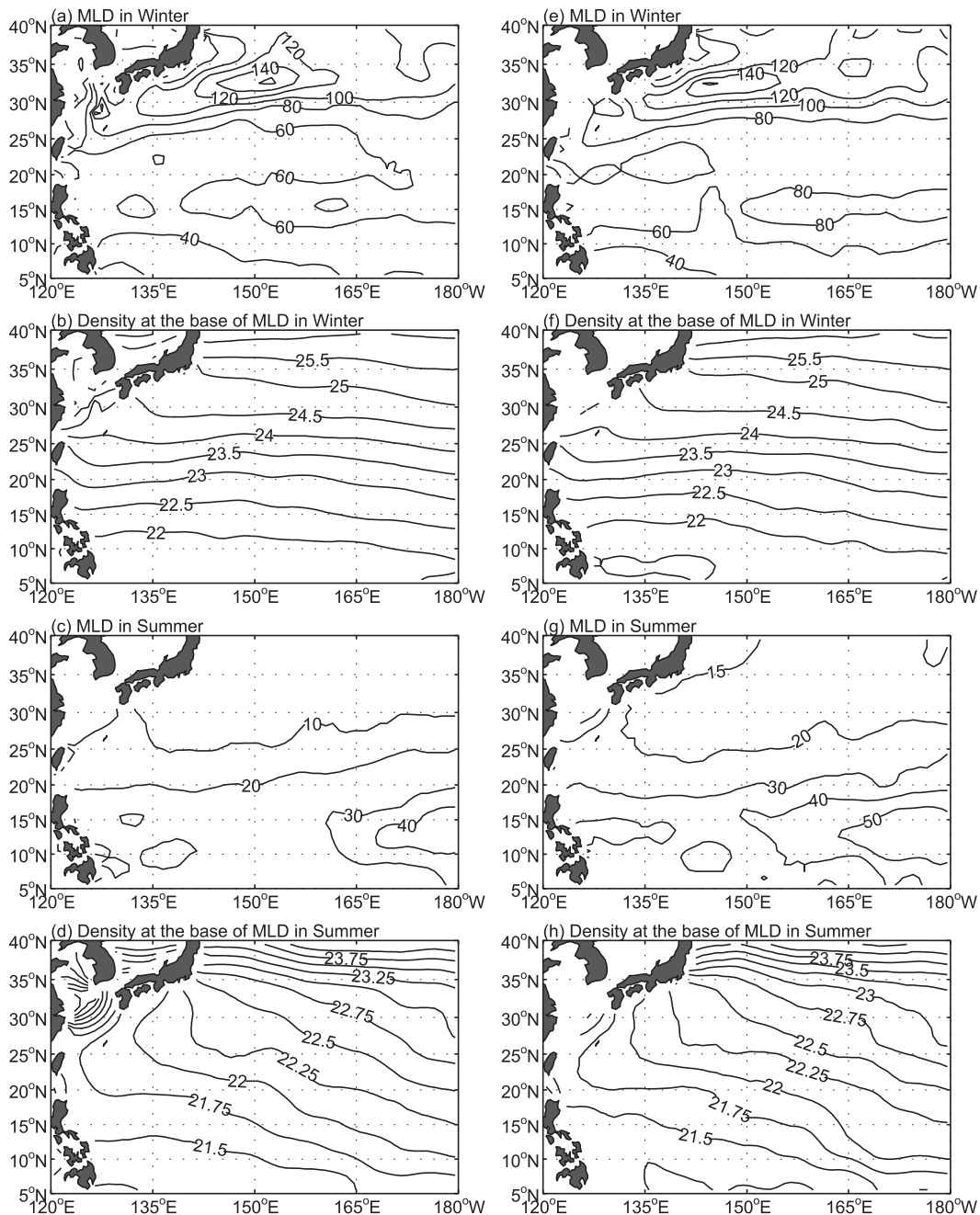


FIG. 3. The depth (m) of the mixed layer in (a) winter (December–February) and (c) summer (July–September). The potential density at the base of the mixed layer in kg m^{-3} in (b) winter and (d) summer based on the WOA09 data; (e)–(h) as in (a)–(d), but for the MOAA-GPV data.

anomalies become progressively weaker with time and move deeper as evidenced by the downward migration of the anomalies ≥ 0.04 PSU. After 2007, the salinity anomalies of negative value ≤ -0.04 begin to penetrate into the permanent thermocline with a descent speed of about 50 m yr^{-1} . This result is consistent with that of Yan et al. (2012), although the depths of the maximum anomalies differ. This difference might be due to the use

of different temperature and salinity data. In addition, this result also resembles the ECCO outputs (Fig. 5), although the ECCO anomalous signals that penetrate into the deeper ocean are weaker.

To provide a synoptic view of the distribution and properties of the upper-ocean salinity changes, the salinity and its anomalies along the meridional section at 135.5°E (averaged over $16^\circ\text{--}30^\circ\text{N}$) and the zonal section

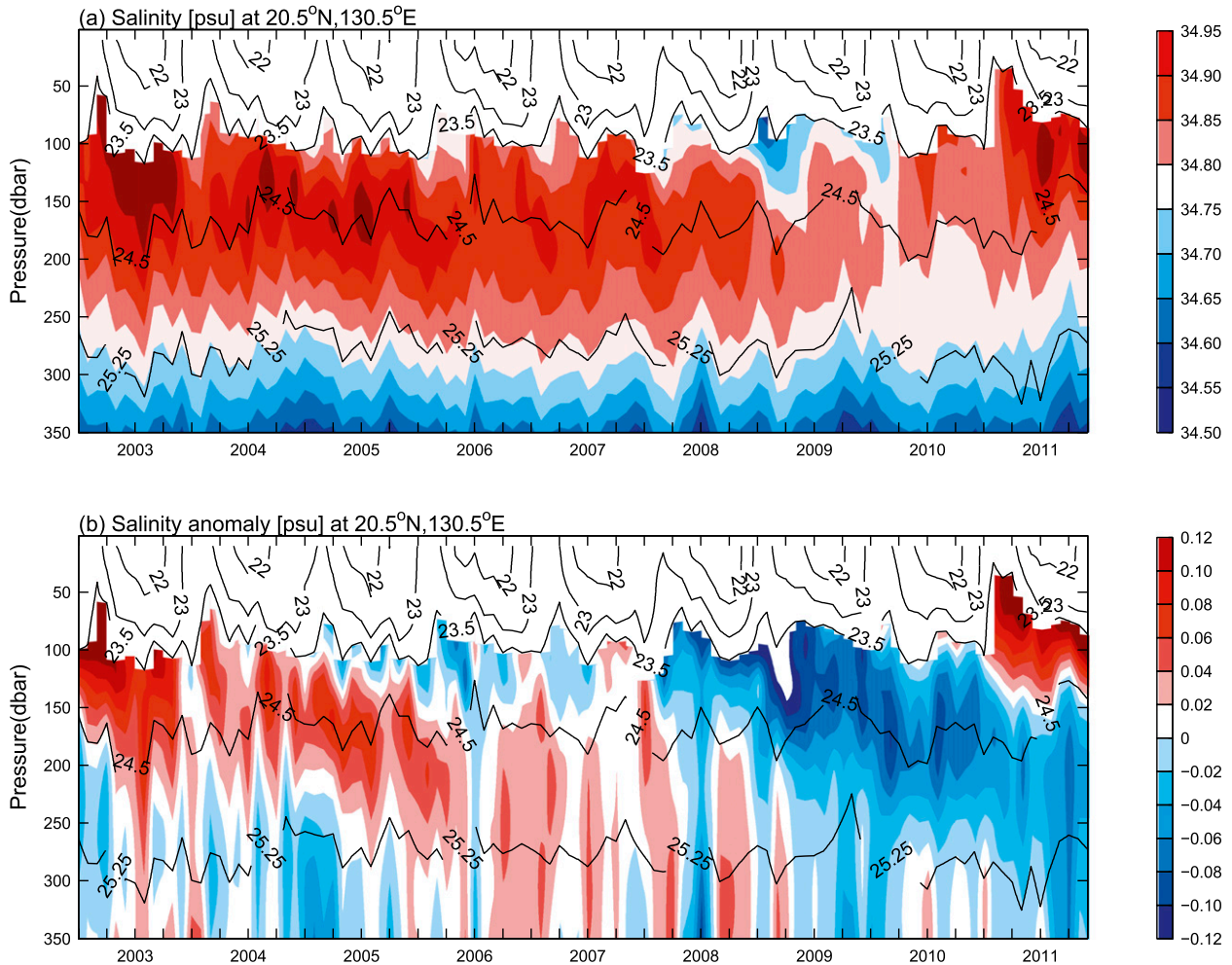


FIG. 4. Pressure–time maps of (a) salinity and (b) salinity anomalies (PSU) at 20.5°N, 130.5°E (see Fig. 2c: blue plus sign) based on the MOAA-GPV data. Also included are the isopycnal surface contours.

at 21.5°N (averaged over 120°–150°E), respectively, are examined (Fig. 6). Similar to the distribution in Fig. 4, the salinity changes along the meridional and zonal sections are primarily confined to the upper 100–250-m depth (or 23.6–25.2 σ_θ). In addition, as noted by Yan et al. (2012), the change of salinity anomalies between 100 and 250 m is approximately twice as strong along the meridional section as along the zonal section, with meridional salinity decreased about 0.2 PSU compared to 0.1 PSU of the zonal section over the period 2003–09, as shown in Figs. 6a and 6b.

To better view how the salinity is distributed horizontally in the layers of the maximum salinity variation from 2003 to 2011, we compute empirical orthogonal functions (EOFs) of salinity anomalies, averaged from 23.6–25.2 σ_θ (nearly 100–250 m). Figure 7 shows the first EOF of salinity anomalies and its corresponding time series. This map displays features similar to those of Li

et al. (2012), except that the salinity anomalies shown here are along the isopycnal surfaces from 23.6–25.2 σ_θ . The first EOF, which explains 49% of the total variance, exhibits a dipole structure with positive sign in the northwest subtropical gyre from 15° to 30°N and negative sign in the tropical region (from 5° to 15°N). In the tropical region, the strongest amplitude on the order of -0.04 occurs along 10°N, while in the northwest subtropical gyre, the strongest amplitude on the order of 0.03 occurs along the Kuroshio Extension from the coast of Japan to $\sim 150^\circ\text{E}$. The time series of the first EOF, shown in Fig. 7b, exhibits a decreasing tendency, with positive values occurring during 2003–07 and negative values occurring during 2008–11. A similar EOF pattern is also found for the 13-month smoothed (using an FFT-based, 13-month low-pass filter to remove high-frequency variability) salinity anomalies field, although the region of strongest salinity change becomes smaller in the

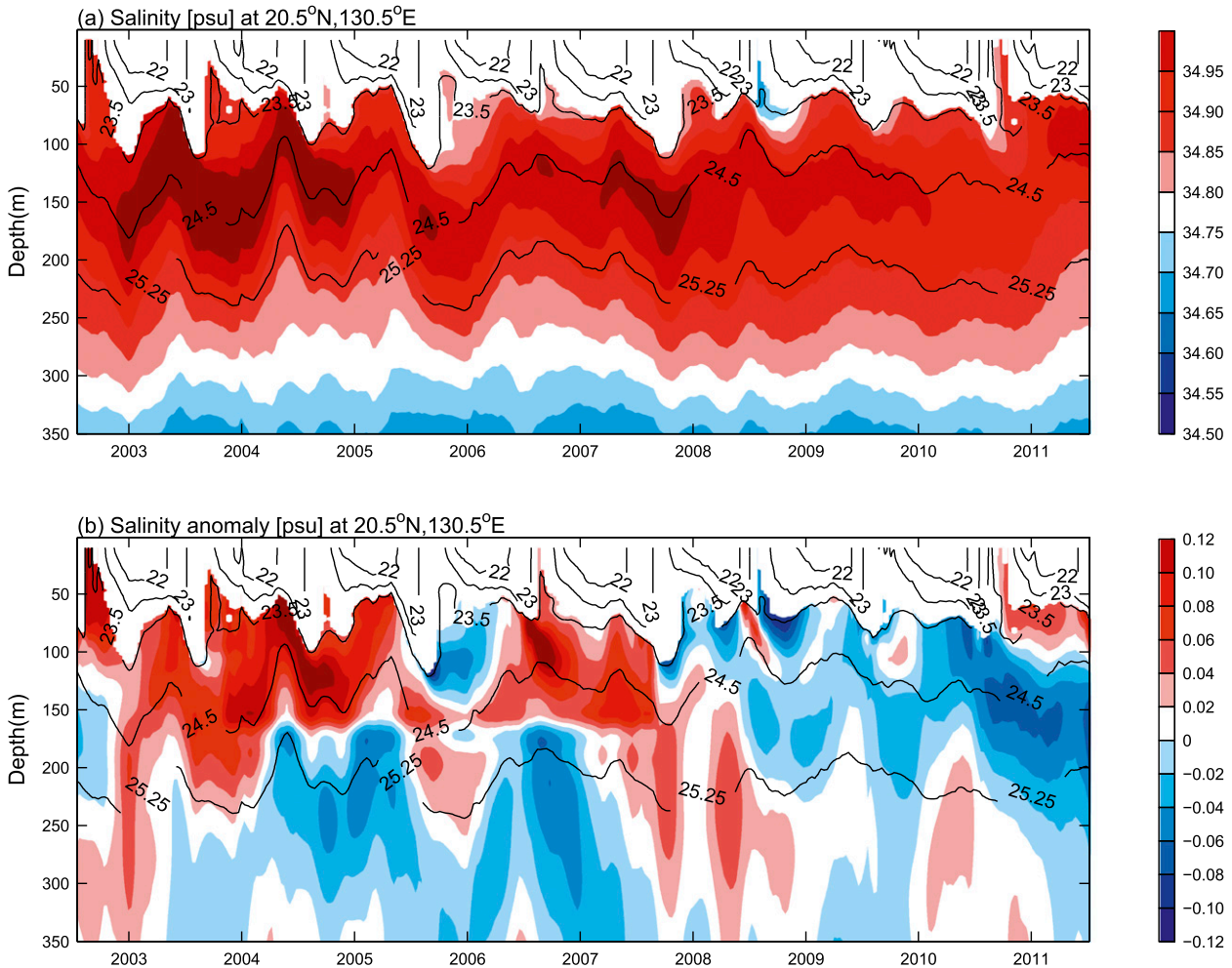


FIG. 5. As in Fig. 4, but for the ECCO data.

northwest subtropical gyre (cf. Figs. 7a,c). The consistent structure among our Figs. 4–7 and the figures of Li et al. (2012) and Yan et al. (2012) suggests that subsurface waters from 23.6 to $25.2 \sigma_\theta$ in the northwest subtropical gyre freshen over the period 2003–11. In addition, the region of strongest freshening is roughly coincident with the area of the strongest subduction in the northwest subtropical gyre (Qiu and Huang 1995; Liu and Huang 2012), suggesting a possible connection between the subsurface freshening and the subduction of surface anomalies.

4. Generation mechanism of the subsurface salinity anomalies

a. The observed salinity anomaly subduction from the surface to the thermocline

Now we turn to the relationship between salinity anomalies at the surface and those at depth. Figure 8

shows a bar graph of salinity anomalies at selected depths averaged over the region of the northern lobe of the EOF dipole in Fig. 7. Note that the interannual variations are prominent in the near surface (10 m), and this variability survives into the interior (see Fig. 8). The progressive delay in the onset of anomalies with depth is also clear, especially for the negative anomalies (note the time of the first zero crossing after 2007 at each depth). A significant feature of the plot is the attenuation of the amplitude of the salinity anomalies as they deepen. The time-delay plot of Fig. 8 suggests that the salinity anomalies propagate from the surface to the main thermocline, in agreement with the results of Figs. 4–6.

Figure 9 illustrates the latitude–depth propagation of the anomalies, showing the history of the salinity anomalies averaged over the longitude band of 125° – 150° E. Each of the panels in Fig. 9 shows a 1.5-yr-long time average over the zonal extent of the domain. The earliest plots (Figs. 9a–c) show the movement of a positive

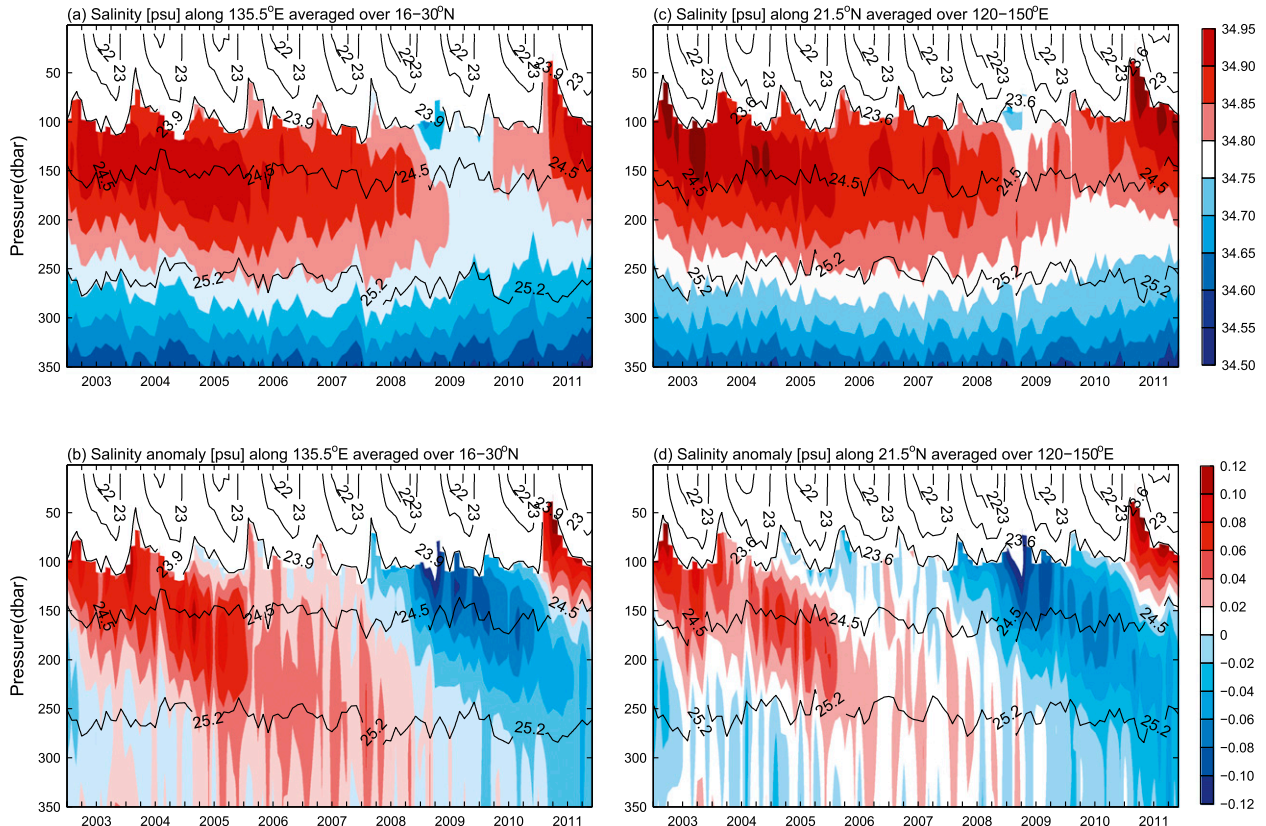


FIG. 6. As in Fig. 4, but for along 21.5°N and 135.5°E (see Fig. 2c: blue intersecting lines).

salinity anomaly downward from the surface to 300 m, while the latter (Figs. 9d–f) show a negative anomaly following a similar trajectory. Along with the deepening comes a southward displacement, consistent with signal propagation along isopycnals.

To obtain a more comprehensive basinwide picture of the propagation pathways, we apply the technique used by van der Werf et al. (2009) and van Sebille et al. (2011) and evaluate lagged correlations of the salinity anomalies. We choose a reference location (20° – 23°N , 125° – 130°E ; i.e., the blue rectangle in Fig. 10) and calculate lagged correlations between the anomaly at this location and those at all other points. This effectively tracks the origin and pathway of the salinity anomalies in the upper ocean. The reference region was selected because it is situated downstream, where the waters may be expected to reenter the Kuroshio (Wyrtki 1975; Reid 1997; Talley et al. 2011). The correlation value r is then calculated as a function of lag and location in the study region. At each location, the lag where r attains its maximum is defined as the most probable lag. For many locations, especially in the eastern and southern Pacific subtropical gyre, the correlation with the referenced point is low and possibly not significant. Thus we show only the

correlations larger than 0.65, which is significantly different from zero at the 95% confidence level ($r = 0.622$) according to a Student's t test. As shown in Fig. 10, the largest correlation to the reference point (20° – 23°N , 125° – 130°E) is found in the center and vicinity of the reference point, and correlations >0.65 are seen in most of the northwest Pacific subtropical gyre. In addition, a tongue of high correlation (≥ 0.80) from the outcrop zone [$\sim(25^{\circ}$ – 35°N , 140° – $160^{\circ}\text{E})$] to the southern rim ($\sim 15^{\circ}\text{N}$) of the northwest subtropical gyre is also found, approximately following the geostrophic streamlines. The successive decreasing of the time lag (~ 1 yr) moving southwestward from outcrop zone to the east of Luzon Strait ($\sim 15^{\circ}\text{N}$) suggests a direct propagation pathway of salinity anomalies along this tongue. This lag time is consistent with that of subtropical mode water, which is subducted in the south of the Kuroshio between 132°E and near the date line, and advected southwestward by the Kuroshio Countercurrent to the western boundary (Oka 2009; Oka and Qiu 2012).

To further examine the propagation characteristics of salinity anomalies, we use a Hovmöller diagram, as shown in Fig. 11, with a focus along the tongue of high correlation ($r \geq 0.80$, as marked in Fig. 10). Contours on this plot

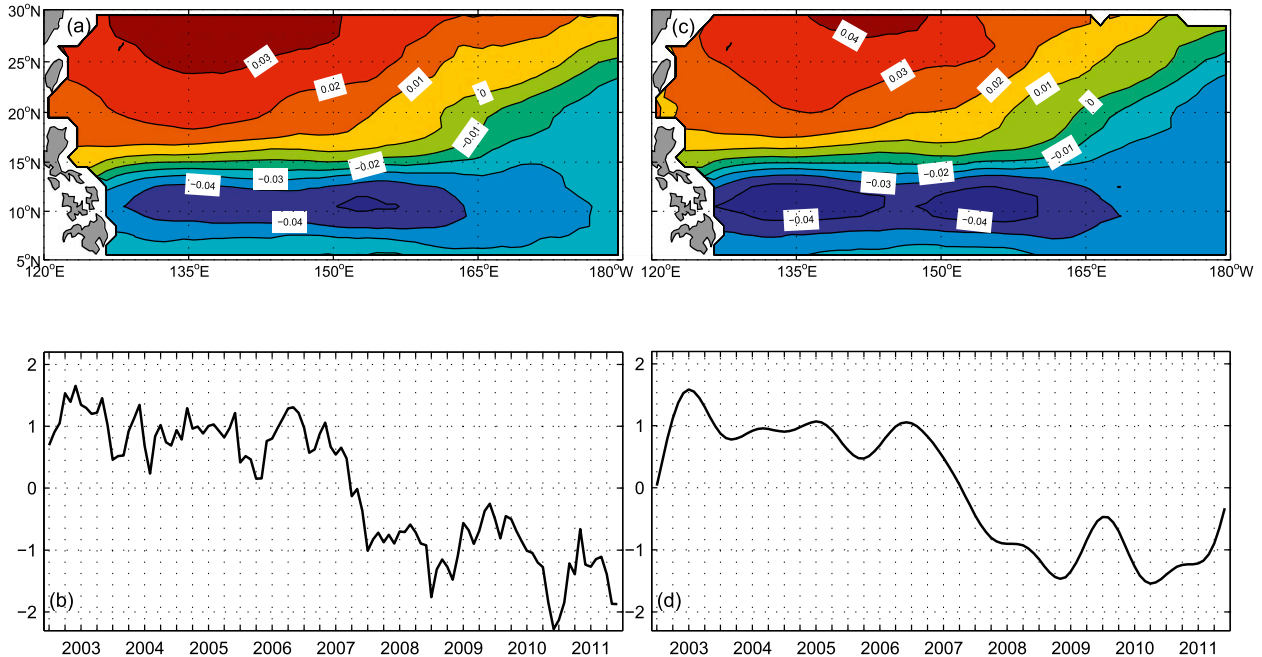


FIG. 7. (a) The first EOF mode of salinity anomalies between 23.6 and 25.2 σ_θ , which explains 49% of the total variance based on the MOAA-GPV data; (b) the associated time series. (c),(d) As in (a),(b), but for the first EOF mode of the salinity field, which has been smoothed using a 13-month low-pass filter to remove the intra-annual variability and highlight the interannual variability. The EOF of (c) explains 51% of the variance.

are of the average depth of the isopycnal range from 24.5–25.2 σ_θ . The latitude–time plot of the anomalies shows that the signals first generate at the outcrop zone (30°–35°N) and then travel deeper and southward to the east of Luzon Strait (~15°N). The coherent movement of the anomalies from the outcrop zone southward into the interior along isopycnals shows that subsurface salinity anomalies in the east of Luzon Strait are mainly dominated by the surface salinity anomalies in the outcrop zone.

b. A predictive model of anomalies transfer from surface to the thermocline

To understand the subduction (Iselin 1939; Stommel 1979) of salinity anomalies from the surface to the permanent thermocline along isopycnals, we follow the work of Nonaka and Sasaki (2007) and Laurian et al. (2009) and project salinity on the time-varying isopycnal surfaces. Assuming weak turbulent mixing across density interfaces, water mass transfer from the surface to the permanent thermocline is quasi-adiabatic ($dT_\sigma = 0$). Thus, the thermocline salinity is a lagged expression of the surface salinity, that is,

$$TS_\sigma(t) = SSS_\sigma(t - t_0), \quad (1)$$

where TS_σ and SSS_σ are the salinity at the permanent thermocline and the surface along the isopycnal σ ,

respectively. The quantity t_0 is the time taken by salinity to travel from the surface to the permanent thermocline. The corresponding salinity anomalies of thermocline TSA_σ and surface $SSSA_\sigma$ can be defined as

$$\begin{cases} TSA_\sigma(t) = TS_\sigma(t) - \overline{TS}_\sigma(t) \\ SSSA_\sigma(t - t_0) = SSS_\sigma(t - t_0) - \overline{SSS}_\sigma(t - t_0), \end{cases} \quad (2)$$

where the overbar represents climatological monthly means. Combining Eq. (1) and Eq. (2), the thermocline salinity anomalies can be written

$$TSA_\sigma(t) = SSSA_\sigma(t - t_0) + \overline{SSS}_\sigma(t - t_0) - \overline{TS}_\sigma(t). \quad (3)$$

Since the location of isopycnal outcrop is frequently influenced by local heat and freshwater flux variability (Nonaka and Sasaki 2007; Laurian et al. 2009; Durack and Wijffels 2010), the displacement (dy) of the isopycnal outcrops with respect to their monthly means over the study period can be given as

$$dy = -\frac{SSD(t - t_0) - \overline{SSD}(t - t_0)}{|\nabla \overline{SSD}(t - t_0)|}, \quad (4)$$

where SSD is the sea surface density, \overline{SSD} is the mean sea surface density over the study period, and $\nabla = (\partial/\partial x, \partial/\partial y)$ is the normal horizontal derivative operator. Equation (4)

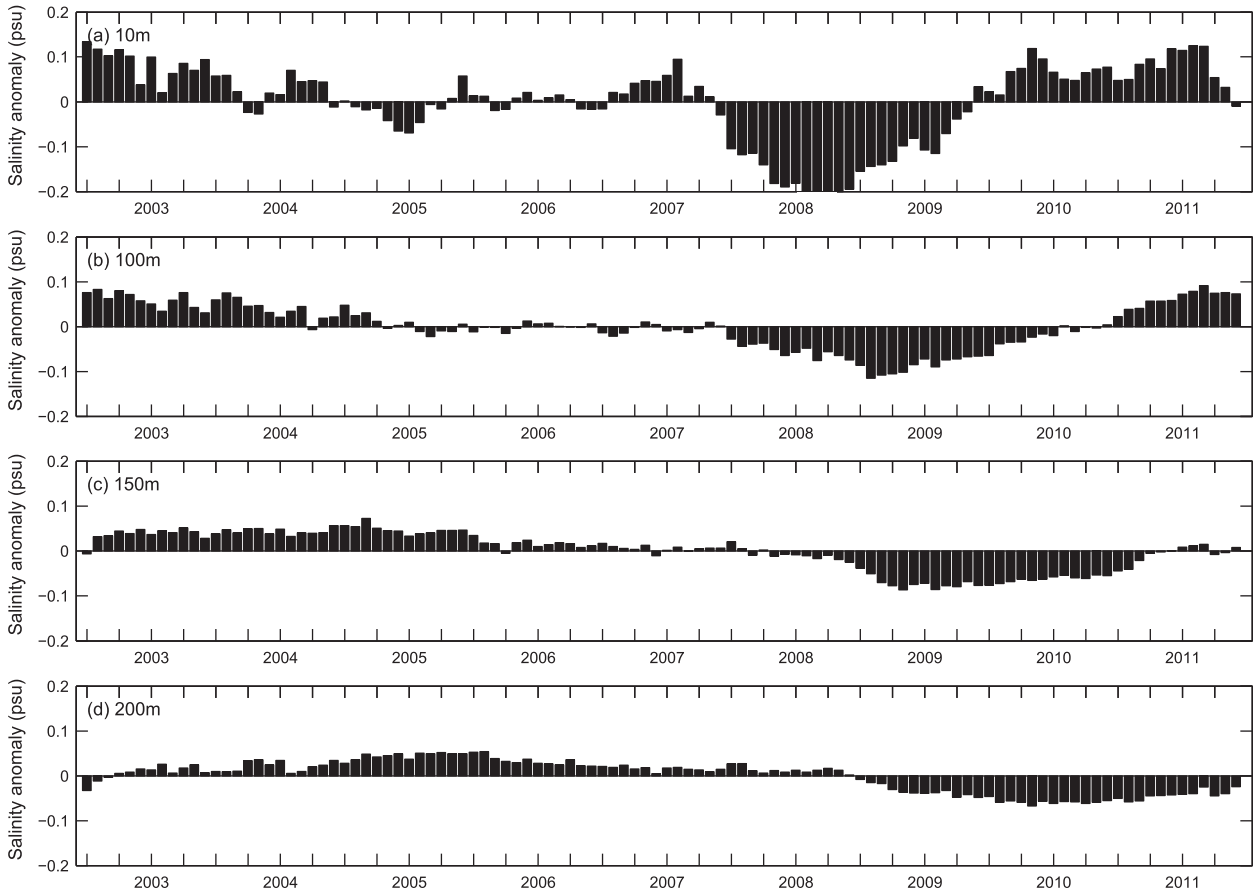


FIG. 8. Variations of salinity anomalies at selected layers: (a) 10, (b) 100, (c) 150, and (d) 200 m for the region (16°–30°N, 125°–150°E) based on the MOAA-GPV data. The region was selected based on the EOF analysis in Fig. 7. The 18-month time periods are used for calculating the positive and negative salinity anomalies in Fig. 9.

is essentially the same as Eq. (2) of Nonaka and Sasaki (2007) and Laurian et al. (2009). Combining Eqs. (1) and (4) expresses the mean thermocline salinity in terms of the mean surface salinity as

$$\overline{TS}_\sigma(t) = \overline{SSS}_\sigma(t - t_0) + dy(t - t_0) \cdot |\nabla SSS_\sigma(t - t_0)|. \quad (5)$$

By combining Eq. (3) and Eq. (5), we obtain the following expression for the salinity anomalies in the thermocline

$$TSA_\sigma(t) = SSSA_\sigma(t - t_0) - dy(t - t_0) \cdot |\nabla SSS_\sigma(t - t_0)|. \quad (6)$$

Equation (6) is the prediction of subsurface salinity anomalies that transfer from the surface along any given isopycnal surface. In Eq. (6), the first term of the right-hand side indicates the direct effect of local surface salinity anomalies; the second term denotes the migration-driven change, which is modified by the surface salinity field and the migration of the outcrop lines. Because the

meridional gradients in the salinity field are very strong in the outcrop region (Fig. 2), the migrating outcrops will carry the surface signals into the ocean interior by subduction. For example, when the outcrop lines migrate to a higher (lower) salinity zone, more (less) saline waters are subducted. This formulation is closely related to that used by Nonaka and Sasaki (2007) and Laurian et al. (2009) for the temperature and/or salinity anomalies associated with horizontal and vertical displacement of the isopycnal surface.

Having established the expressions for the connection between the surface and thermocline salinity anomalies [Eqs. (2) and (6)], we now evaluate these expressions with the MOAA-GPV observed data and the ECCO-simulated data to understand the subduction of salinity anomalies from the surface to the permanent thermocline. Figure 12 shows the distributions of the observed, simulated and predicted TSA on the 24.5–24.8- σ_θ surface in March 2004 by Eqs. (2) and (6). We first use March 2004 as an example because of its strong positive salinity

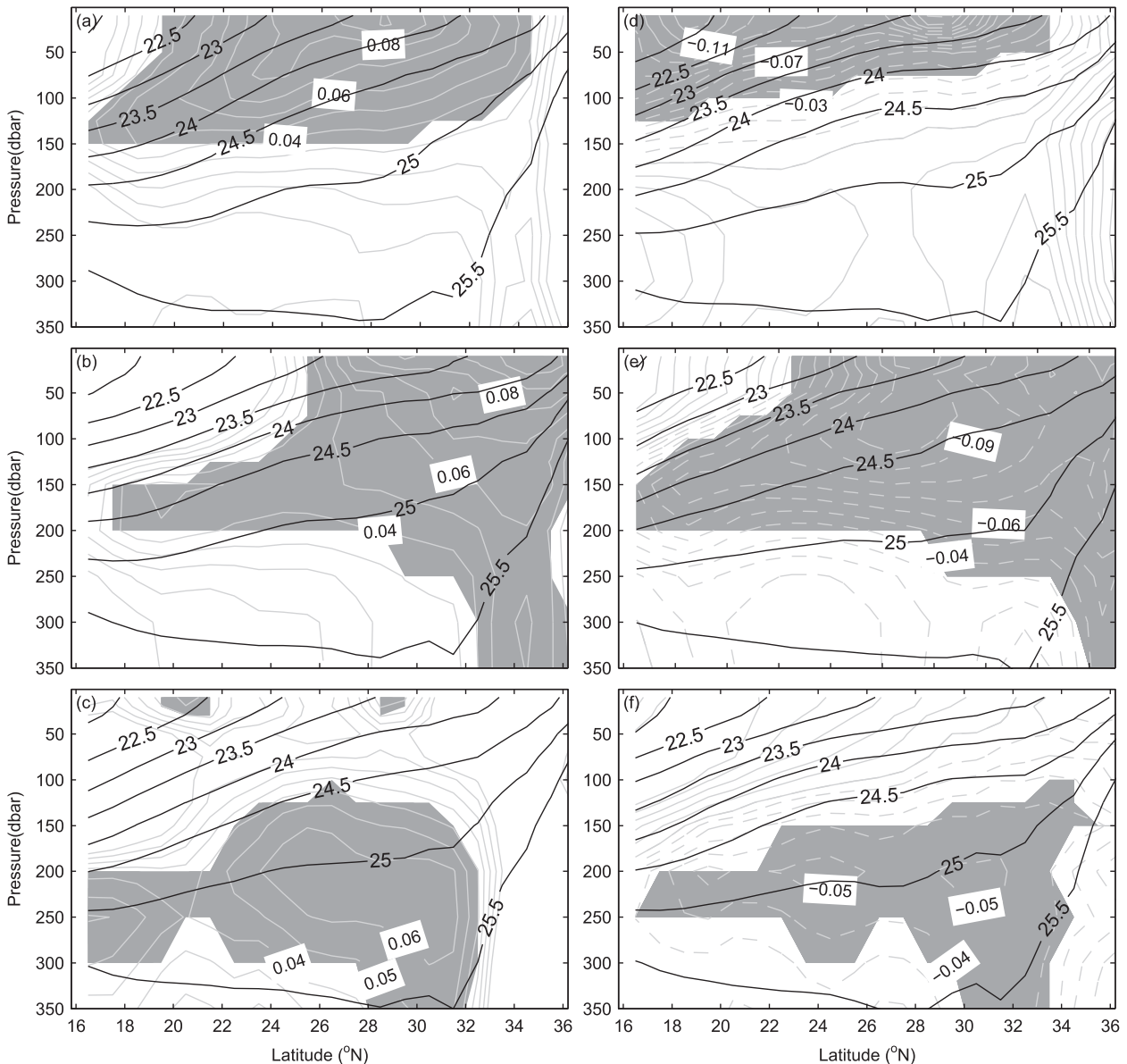


FIG. 9. Salinity anomalies [positive (negative) gray solid (dashed) lines] as a function of depth and latitude averaged over the longitude band 125° – 150° E with corresponding mean potential density contours superimposed (solid black lines) over the 18-month time periods: (a) January 2003–June 2004; (b) July 2004–December 2005; (c) January 2006–June 2007; (d) July 2007–December 2008; (e) January 2009–June 2010; and (f) July 2010–December 2011. Anomalies >0.03 PSU and <-0.03 PSU are shaded. Note that the anomalies ($\times 2$ PSU) for the period January 2006–June 2007 are shown for clarity. These plots are based on the MOAA-GPV data.

anomalies in the outcrop zone (see Fig. 5, Fig. 6, and Fig. 11). The spatial distribution of the predicted TSA (Figs. 12a,c) in March 2004 is consistent with that of the observed and simulated TSA (Figs. 2b,d), although some biases exist in amplitude. We attribute the distinctions to the lack of diapycnal mixing and dissipation in the prediction [Eq. (6)]. As shown in Fig. 12a, positive TSA with high values occurring in the high correlation zone (>0.65 ; Fig. 10) are predicted and are in agreement with the

positive TSA observed by Argo (Fig. 12b). These anomalies are clearly advected by the mean flow from the subtropics. Although differences exist, the spatial distribution of the predicted TSA in March 2004 also agrees with the ECCO-simulated results in the northwest Pacific subtropical gyre (Figs. 12c,d). In addition, negative TSA appearing in the high correlation zone for March 2009 are also shown in Fig. 13. The distributions of negative anomalies for the prediction are

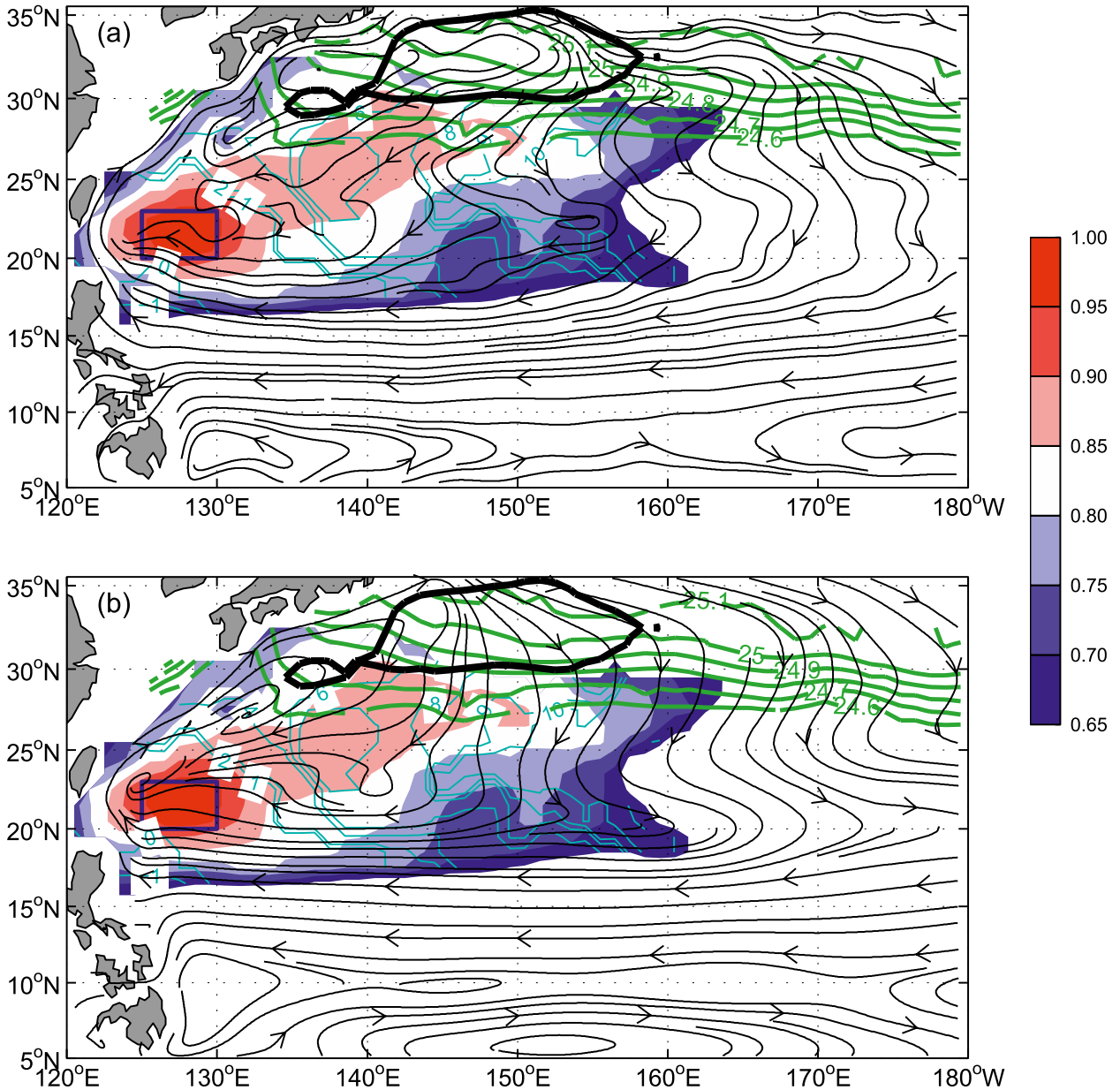


FIG. 10. The correlation coefficients ($r \geq 0.65$) between the salinity anomalies in the northwest Pacific and that in the index zone (blue rectangle: 20°–23°N, 125°–130°E) on $24.5\text{--}25.2\sigma_\theta$ (color shading). The lags of 10, 9, 8, 6, 4, 2, 1, 0, and -1 months are shown by the cyan lines. The late-winter (January–March) mean outcrop lines of $24.6\text{--}25.1\sigma_\theta$ and MLD of 190 m are shown by the green and solid black lines, respectively. The streamlines (black arrow) of (a) the mean geostrophic velocity from MDT_CNES-CLS09 (Rio et al. 2011) and (b) the near-surface velocity field ($22\text{--}25.2\sigma_\theta$) from ECCO averaged over the study period are shown. The geostrophic velocity field has been smoothed using a 5-point moving-average filter.

similar to those of observation and simulation, consistent with the results of positive anomalies propagation along the isopycnals.

To display the overall features of the predicted, observed, and simulated TSA over the study period, we compute mean salinity anomalies averaged over the main propagation region marked in Fig. 10. Note that since

strong subduction mainly takes place in late winter, the terms on the right side of Eq. (6) are considered only for the winter months from January–March. The results are shown in Fig. 14. In general, the interannual variability of the predicted salinity anomalies is similar to those of the observations and simulations. Positive anomalies occur over the period 2003–07 and are near zero in 2008,

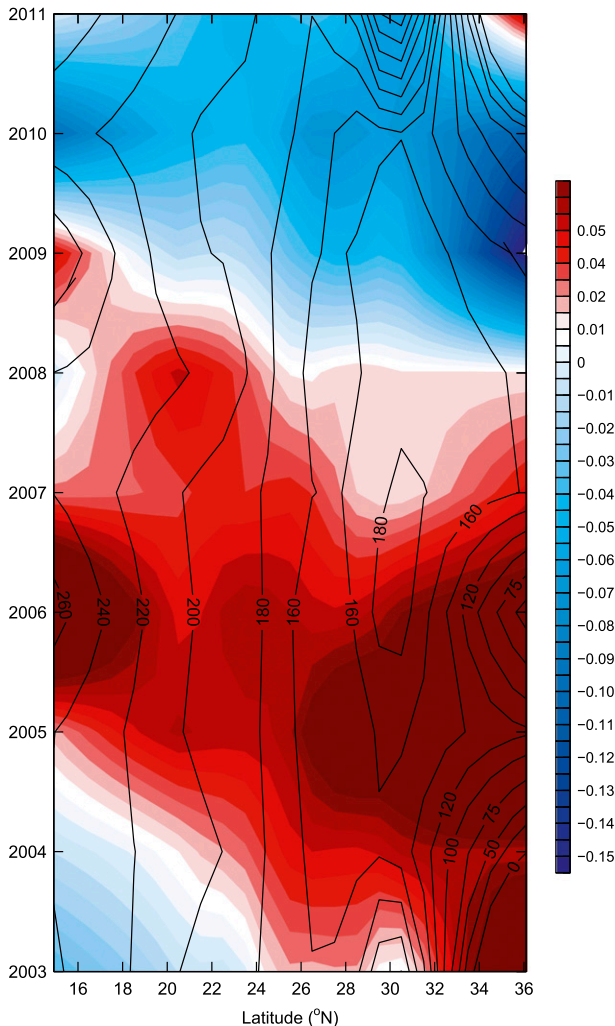


FIG. 11. Zonal-average salinity anomalies (color shading) along $24.5\text{--}25.2\text{-}\sigma_{\theta}$ isopycnals and the mean depths of corresponding isopycnals (contours) during late winter (January–March) in the region with a correlation >0.8 .

although some discrepancies are seen. The salinity anomalies continue to decrease with time and return to near zero in 2011. These results are consistent with the above observational analyses, suggesting that thermocline salinity anomalies in the northwest Pacific subtropical gyre are mainly dominated by the surface anomalies.

5. Summary and discussion

At the western boundary, the NEC bifurcates into the northward Kuroshio and equatorward Mindanao Current. As a conservative tracer, surface salinity anomalies subducted in the northeast/central subtropical Pacific are expected to propagate southward and then westward along the NEC before splitting into northward and

equatorward components. The equatorward portion may enter the Indian Ocean via the Indonesian Throughflow (Stammer et al. 2008) or affect the thermocline temperature and salinity structure of the equatorial region (Lukas 2001; Fukumori et al. 2004).

At the northern downstream region, the subsurface salinity variability in the northwest Pacific could be attributed to the variability of the northeast/central subtropical Pacific via the Kuroshio. However, the observed data show that anomalies of surface subducted salinity in the northeast/central subtropical north Pacific become very small when reaching the western Pacific ($145^{\circ}\text{--}170^{\circ}\text{E}$) because of intensive along-path dispersion (Sasaki et al. 2010; Li et al. 2012). This result is consistent with that of Yan et al. (2012), who showed that salinity advection via the Kuroshio cannot account for the variability of salinity anomalies in the east of Luzon Strait. As shown in Figs. 4–7, a prominent freshening of subsurface salinity in the northwest Pacific is observed over the period 2003–11. In addition, a bar graph of salinity anomalies at selected depths provides the visual impression that salinity anomalies propagate from the surface to the main thermocline (Fig. 8). Lag correlations, Hovmöller diagrams, and predictive models support this result and suggest that the subsurface salinity anomalies do originate from the surface outcrop region of $25^{\circ}\text{--}35^{\circ}\text{N}$, consistent with the classic late-winter subduction mechanism. Our results, however, differ from those of Kessler (1999), who examined repeated CTD sections spanning the equator along 165°E during the period 1984–97. He found that, although much of the salinity change on the $24.5\text{-}\sigma_{\theta}$ surface could be attributed to zonal advection along the isopycnal, the surface subduction is not the only process affecting isopycnal salinity variations in the southeastern Pacific. Why the southern Pacific is different in this respect from the northern Pacific is not clear.

By analyzing the salinity along 137°E during the last few decades of the last century (1967–95), Suga et al. (2000) found that local surface forcing could not explain the observed salinity anomalies from 13° to 27°N . These results are consistent with ours, and it is necessary to look at the remote surface salinity anomalies in the outcrop region to explain the downstream isopycnal variations in the northwest Pacific subtropical gyre. As shown in Fig. 15, the sign of surface salinity anomalies in the outcrop region is in good agreement with that on the isopycnals. During the period 2003–11, the entire outcrop region becomes colder and fresher, consistent with the fresher water observed with a lag in the northwest Pacific.

The propagation of salinity anomalies in the thermocline is the result of subduction (Stommel 1979; Luyten et al. 1983). The anomalies are created as the result of

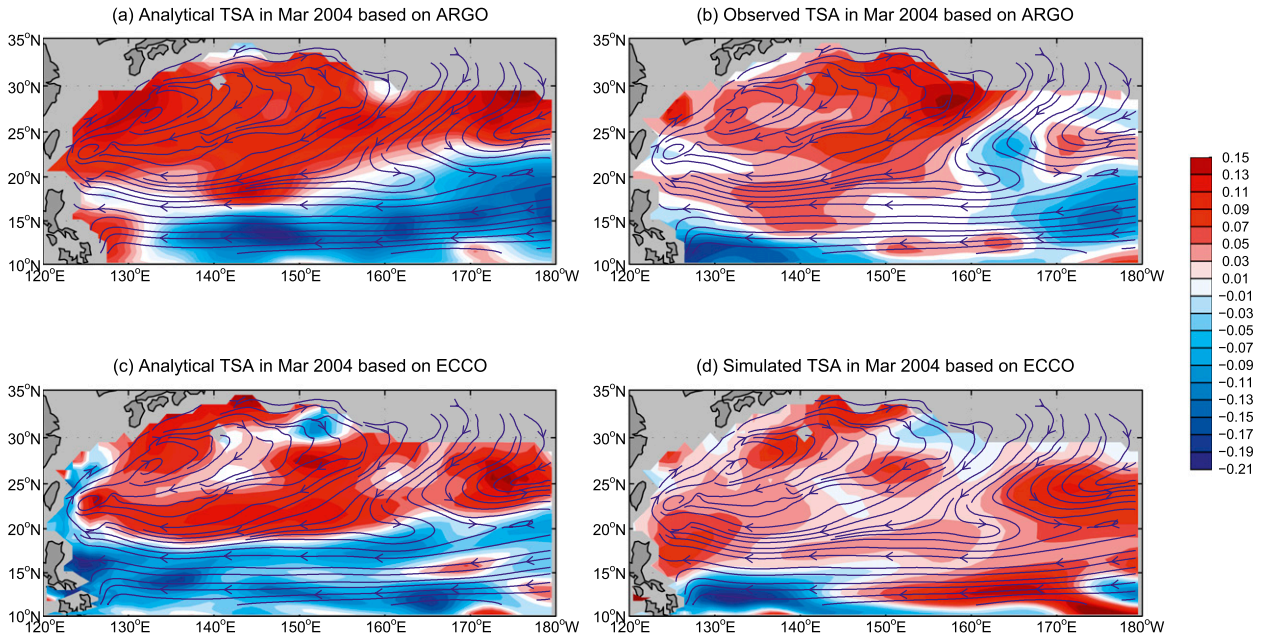


FIG. 12. (a) Salinity anomalies predicted by Eq. (6) on $24.5\text{--}24.8\text{-}\sigma_\theta$ isopycnal surfaces for March 2004 based on the MOAA-GPV data; (b) as in (a), but for the observed anomalies estimated using Eq. (2); (c),(d) as in (a),(b), but for ECCO outputs. In all panels, the streamlines for January 2004 are shown with blue arrows based on ECCO outputs and the lagged time t_0 used is 2 months. The velocity field has been smoothed using a 2-point moving-average filter.

coupled air–sea interactions in the mixed layer of the outcrop zone and are advected along isopycnals. The main dynamical quantity emphasized in subduction studies is potential vorticity (PV), which is materially

conserved and hence a useful marker of the pathway of water masses. In the present study, we map the monthly mean PV on the $24.5\text{-}\sigma_\theta$ isopycnal surface to see if one can track the propagation pathway of the salinity anomalies

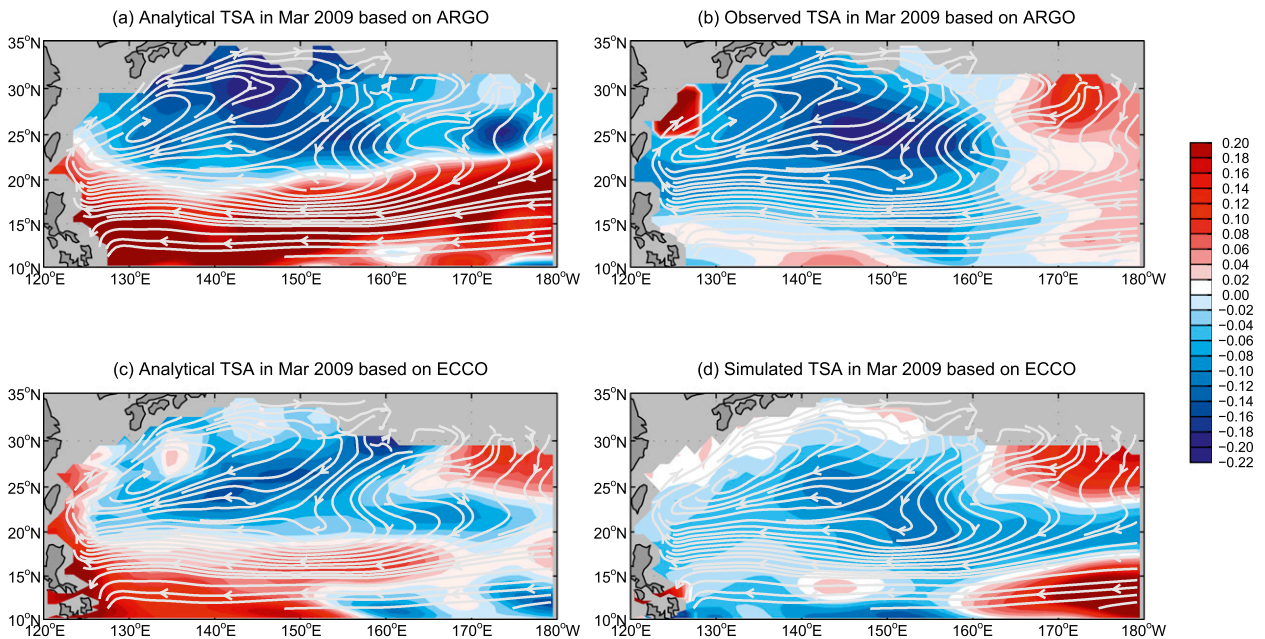


FIG. 13. As in Fig. 12, but for the salinity anomalies estimated in March 2009. The streamlines shown here with white arrows are for January 2009 based on ECCO outputs.

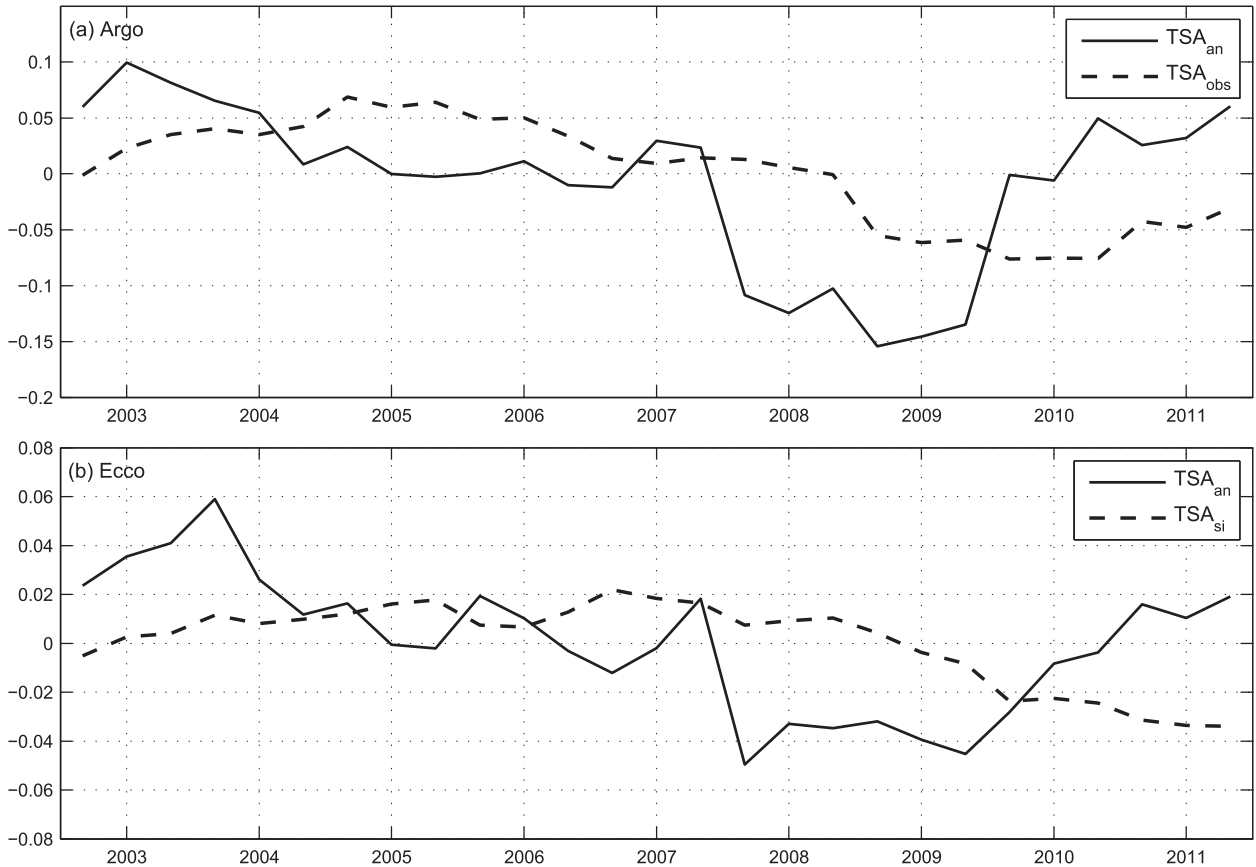


FIG. 14. Salinity anomalies on $\sigma_{\theta} = 24.5\text{--}25.2$ averaged in the region with correlation >0.8 (dashed line) and predicted salinity anomaly isopycnal $\sigma_{\theta} = 24.5\text{--}25.2$ from Eq. (2) (solid line) over the period of 2003–11: (a) based on the MOAA-GPV data and (b) based on the ECCO outputs.

using PV. Here the large-scale PV can be written as $PV = g^{-1}fN^2$ where $N^2 = -(g/\rho_{\theta})\partial\sigma_{\theta}/\partial z$ is the squared buoyancy frequency, f is the Coriolis parameter, and g is the acceleration of gravity. As shown in Fig. 16, the observed low-value ($<5 \times 10^{-11} \text{ m}^{-1} \text{ s}^{-1}$) PV is generated in the

outcrop region and moves southwestward to the deeper ocean. The trajectories of the PV contours are roughly coincident with those of salinity anomalies, suggesting that isopycnal salinity anomalies in the northwest Pacific gyre are generated via surface subduction from the

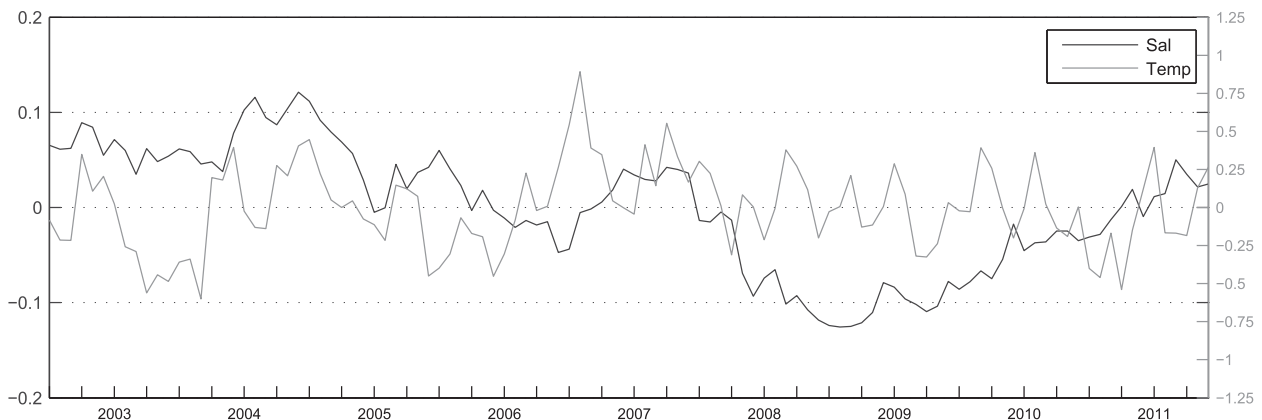


FIG. 15. The mixed layer salinity (light blue lines, PSU) and temperature (dark green lines, °C) anomalies in the region of $30^{\circ}\text{--}35^{\circ}\text{N}$, $120^{\circ}\text{--}150^{\circ}\text{E}$ during the period 2003–11.

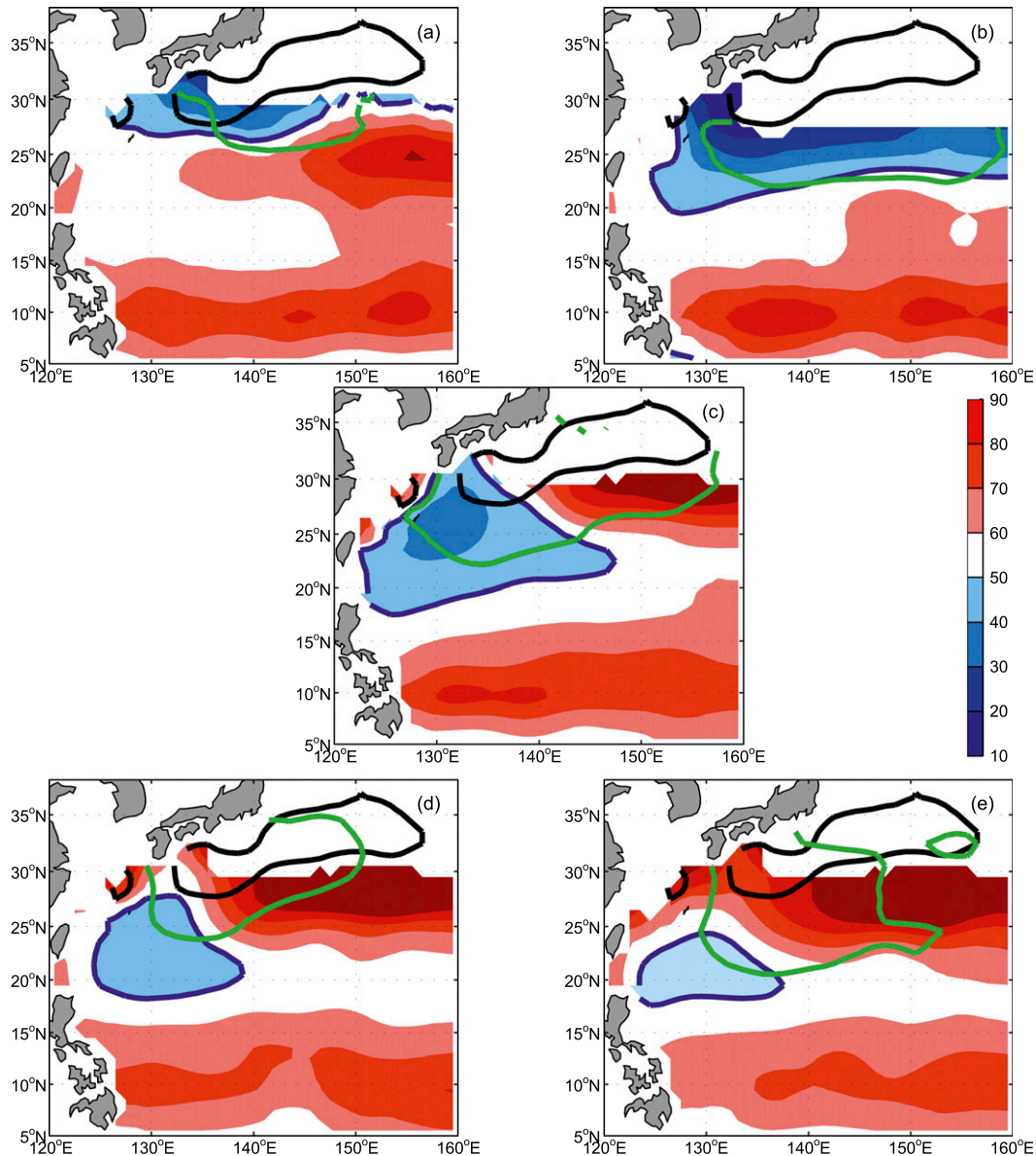


FIG. 16. The multiyear monthly mean PV (colors, $10^{-11} \text{ m}^{-1} \text{ s}^{-1}$) and salinity anomalies of 0.05 PSU (green lines) in (a) January, (b) March, (c) May, (d) July, and (e) September along $24.5\text{-}\sigma_{\theta}$ isopycnal surfaces during the period 2003–06. The months of January, March, May, July, and September are chosen based on the results of about 1-yr lead time from the outcrop region to the latitude of 15°N . Positive anomalies during the period 2003–06 rather than all anomalies of 2003–11 are considered here. The maximum MLDs of 150 m in January are plotted as black solid lines.

outcrop region and then spread southwestward, approximately following the mean flow.

To summarize, this paper presents a comprehensive study on the variation of the subsurface salinity anomalies and their generation mechanism in the northwest Pacific subtropical gyre using a combination of a gridded monthly dataset of temperature and salinity obtained from Argo floats and CTDs, ECCO outputs, and a simple predictive model. A prominent freshening with salinity

decreasing about 0.25 PSU is found at depth of about 150 m, and propagates to deeper depths during the period 2003–11 in the northwest Pacific subtropical gyre. The observational and model analyses suggest that the isopycnal salinity anomaly in the northwest Pacific subtropical gyre is the result of surface forcing and late-winter subduction at the outcrop zone [$\sim(25^{\circ}\text{--}35^{\circ}\text{N}, 130^{\circ}\text{--}150^{\circ}\text{E})$]. The salinity anomalies with a decreasing trend are generated in the outcrop region and then

propagate southwestward along with potential vorticity anomalies to the east of Luzon Strait (latitude of $\sim 15^{\circ}\text{N}$ and depth of 240–260 m, Fig. 11), therefore freshening the local water masses, consistent with climatological distribution of potential density and salinity variability at 250 m (Figs. 2c,f). As the anomalies reach the east of Luzon Strait, they tend to turn and travel eastward toward the central Pacific probably via an eastward flow on the equator side of the subtropical gyre (STCC; Uda 1955; Uda and Hasunuma 1969; Qiu 1999; Chu et al. 2002; Kobashi and Xie 2012). Since the relationship between the eastward-propagated anomalies and STCC has not been examined, it cannot be said with certainty that STCC has an influence on the propagation of subduction salinity along the isopycnals, but the present results suggest that continuous forcing of the east of Luzon Strait by salinity anomalies mainly originates from the northwest Pacific subtropical region.

Acknowledgments. We thank the JPL ECCO team for providing the Kalman filter assimilation product. Thanks are also given to the anonymous reviewers for their constructive and helpful comments. This work is partly supported by the National Basic Research Program of China (2011CB403504; 2013CB430301) and the National Natural Science Foundation (NSF) of China (41276025). EPC is supported by ONR Contract N00014-09-1-0587. WKD is supported by NSF Grants OCE-100090 and OCE-100743. This work was performed at COAPS on a Chinese Academy of Science Overseas Fellowship.

REFERENCES

- Antonov, J. I., and Coauthors, 2010: *Salinity*. Vol. 2, *World Ocean Atlas 2009*, S. Levitus, Ed., NOAA Atlas NESDIS 69, 184 pp.
- Balaguru, K., P. Chang, R. Saravanan, L. R. Leung, Z. Xu, M. Li, and J. S. Hsieh, 2012: Ocean barrier layers' effect on tropical cyclone intensification. *Proc. Natl. Acad. Sci. USA*, **109**, 14 343–14 347.
- Bindoff, N. L., and J. A. Church, 1992: Warming of the water column in the southwest Pacific Ocean. *Nature*, **357**, 59–62.
- Bryden, H. L., E. L. McDonagh, and B. A. King, 2003: Changes in ocean water mass properties: Oscillations or trends. *Science*, **27**, 2086–2088.
- Chen, J., T. Qu, Y. N. Sasaki, and N. Schneider, 2010: Anti-correlated variability in subduction rate of the western and eastern North Pacific Oceans identified by an eddy-resolving ocean GCM. *Geophys. Res. Lett.*, **37**, L23608, doi:10.1029/2010GL045239.
- Chu, P. C., R. Li, and X. You, 2002: Northwest Pacific subtropical countercurrent on isopycnal surface in summer. *Geophys. Res. Lett.*, **29**, 1842, doi:10.1029/2002GL014831.
- Deser, C., M. A. Alexander, and M. S. Timlin, 1996: Upper-ocean thermal variations in the North Pacific during 1970–1991. *J. Climate*, **9**, 1840–1855.
- Durack, P. J., and S. E. Wijffels, 2010: Fifty-year trends in global ocean salinities and their relationship to broad-scale warming. *J. Climate*, **23**, 4342–4362.
- Fukumori, I., T. Lee, B. Cheng, and D. Menemenlis, 2004: The origin, pathway, and destination of Niño-3 water estimated by a simulated passive tracer and its adjoint. *J. Phys. Oceanogr.*, **34**, 582–604.
- Gu, D., and S. G. H. Philander, 1997: Interdecadal climate fluctuations that depend on exchanges between the tropics and extratropics. *Science*, **275**, 805–807.
- Halkides, D. J., and T. Lee, 2009: Mechanisms controlling seasonal-to-interannual mixed layer temperature variability in the southeastern tropical Indian Ocean. *J. Geophys. Res.*, **114**, C02012, doi:10.1029/2008JC004949.
- Hosoda, S., T. Ohira, and T. Nakamura, 2008: A monthly mean dataset of global oceanic temperature and salinity derived from Argo float observations. *JAMSTEC Rep. Res. Dev.*, **8**, 47–59.
- Iselin, C. O. D., 1939: The influence of vertical and lateral turbulence on the characteristics of the waters at mid-depths. *Trans. Amer. Geophys. Union*, **20**, 414–417.
- Johnson, G. C., and A. H. Orsi, 1997: Southwest Pacific Ocean water mass changes between 1968/69 and 1990/91. *J. Climate*, **10**, 306–316.
- Kessler, W. S., 1999: Interannual variability of the subsurface high salinity tongue south of the equator at 165°E . *J. Phys. Oceanogr.*, **29**, 2038–2049.
- Kilpatrick, T., N. Schneider, and E. Di Lorenzo, 2011: Generation of low-frequency spiciness variability in the thermocline. *J. Phys. Oceanogr.*, **41**, 365–377.
- Kim, S. B., T. Lee, and I. Fukumori, 2004: The 1997–1999 abrupt change of the upper ocean temperature in the north-central Pacific. *Geophys. Res. Lett.*, **31**, L22304, doi:10.1029/2004GL021142.
- Kobashi, F., and S. P. Xie, 2012: Interannual variability of the North Pacific Subtropical Countercurrent: Role of local ocean–atmosphere interaction. *J. Oceanogr.*, **68**, 113–126.
- Laurian, A., A. Lazar, and G. Reverdin, 2009: Generation mechanism of spiciness anomalies: An OGCM analysis in the North Atlantic Subtropical Gyre. *J. Phys. Oceanogr.*, **39**, 1003–1018.
- Lee, T., I. Fukumori, D. Menemenlis, and L. L. Fu, 2002: Effects of the Indonesian Throughflow on the Pacific and Indian Oceans. *J. Phys. Oceanogr.*, **32**, 1404–1429.
- Li, Y. L., F. Wang, and F. G. Zhai, 2012: Interannual variations of subsurface spiciness in the Philippine Sea: Observations and mechanism. *J. Phys. Oceanogr.*, **42**, 1022–1038.
- Liu, L. L., and R. X. Huang, 2012: The global subduction/obduction rates: Their interannual and decadal variability. *J. Climate*, **25**, 1096–1115.
- Locarnini, R. A., A. V. Mishonov, J. I. Antonov, T. P. Boyer, H. E. Garcia, O. K. Baranova, M. M. Zweng, and D. R. Johnson, 2010: *Temperature*. Vol. 1, *World Ocean Atlas 2009*, S. Levitus, Ed., NOAA Atlas NESDIS 68, 184 pp.
- Lukas, R., 2001: Freshening of the upper thermocline in the North Pacific subtropical gyre associated with decadal changes of rainfall. *Geophys. Res. Lett.*, **28**, 3485–3488.
- Luo, Y. Y., L. M. Rothstein, R. H. Zhang, and A. J. Busalacchi, 2005: On the connection between South Pacific subtropical spiciness anomalies and decadal equatorial variability in an ocean general circulation model. *J. Geophys. Res.*, **110**, C10002, doi:10.1029/2004JC002655.
- Luyten, J., J. Pedlosky, and H. M. Stommel, 1983: The ventilated thermocline. *J. Phys. Oceanogr.*, **13**, 292–309.
- Maes, C., J. Picaut, and S. Belamari, 2005: Importance of the salinity barrier layer for the buildup of El Niño. *J. Climate*, **18**, 104–118.

- Marshall, J., A. Adcroft, C. Hill, L. Perelman, and C. Heisey, 1997: A finite-volume, incompressible Navier–Stokes model for studies of the ocean on parallel computers. *J. Geophys. Res.*, **102**, 5753–5766.
- McDougall, T. J., 1987: Neutral surfaces. *J. Phys. Oceanogr.*, **17**, 1950–1964.
- Montgomery, R. B., 1938: Circulation in upper layers of southern North Atlantic deduced with use of isentropic analysis. *Pap. Phys. Oceanogr.*, **6**, 1–55.
- Nonaka, M., and H. Sasaki, 2007: Formation mechanism for isopycnal temperature–salinity anomalies propagating from the eastern South Pacific to the equatorial region. *J. Climate*, **20**, 1305–1315.
- Oka, E., 2009: Seasonal and interannual variation of North Pacific subtropical mode water in 2003–2006. *J. Oceanogr.*, **65**, 151–164.
- , and B. Qiu, 2012: Progress of North Pacific mode water research in the past decade. *J. Oceanogr.*, **68**, 5–20.
- Parr, A. E., 1938: Isopycnic analysis of current flow by means of identifying properties. *J. Mar. Res.*, **1**, 133–154.
- Peixoto, J. P., and A. H. Oort, 1992: *Physics of Climate*. American Institute of Physics, 520 pp.
- Pierce, D. W., T. P. Barnett, and M. Latif, 2000: Connections between the Pacific Ocean tropics and midlatitudes on decadal timescales. *J. Climate*, **13**, 1173–1194.
- Qiu, B., 1999: Seasonal eddy field modulation of the North Pacific Subtropical Countercurrent: TOPEX/Poseidon observations and theory. *J. Phys. Oceanogr.*, **29**, 2471–2486.
- , and R. X. Huang, 1995: Ventilation of the North Atlantic and North Pacific: Subduction versus obduction. *J. Phys. Oceanogr.*, **25**, 2374–2390.
- , and S. Chen, 2012: Concurrent decadal mesoscale eddy modulations in the western North Pacific subtropical gyre. *J. Phys. Oceanogr.*, **43**, 344–358.
- Reid, J. L., 1997: On the total geostrophic circulation of the Pacific Ocean: Flow patterns, tracers, and transports. *Prog. Oceanogr.*, **39**, 263–352.
- Ren, L., and S. C. Riser, 2010: Observations of decadal time scale salinity changes in the subtropical thermocline of the North Pacific Ocean. *Deep-Sea Res. II*, **57**, 1161–1170.
- Rio, M. H., S. Guinehut, and G. Larnicol, 2011: New CNES-CLS09 global mean dynamic topography computed from the combination of GRACE data, altimetry, and in situ measurements. *J. Geophys. Res.*, **116**, C07018, doi:10.1029/2010JC006505.
- Sasaki, Y. N., N. Schneider, N. Maximenko, and K. Lebedev, 2010: Observational evidence for propagation of decadal spiciness anomalies in the North Pacific. *Geophys. Res. Lett.*, **37**, L07708, doi:10.1029/2010GL042716.
- Schneider, N., 2000: A decadal spiciness mode in the tropics. *Geophys. Res. Lett.*, **27**, 257–260.
- , 2004: The response of tropical climate to the equatorial emergence of spiciness anomalies. *J. Climate*, **17**, 1083–1095.
- Stammer, D., S. Park, A. Kohl, R. Lukas, and F. Santiago-Mandujano, 2008: Causes for large-scale hydrographic changes at the Hawaii Ocean time series station. *J. Phys. Oceanogr.*, **38**, 1931–1948.
- Stommel, H., 1979: Determination of water mass properties of water pumped down from the Ekman Layer to the geostrophic flow below. *Proc. Natl. Acad. Sci. USA*, **76**, 3051–3055.
- Suga, T., A. Kato, and K. Hanawa, 2000: North Pacific tropical water: Its climatology and temporal changes associated with the climate regime shift in the 1970s. *Prog. Oceanogr.*, **47**, 223–256.
- Talley, L. D., 2002: Salinity patterns. *Encyclopedia of Global Environmental Change*, Vol. 1, Wiley, 11 pp.
- , G. L. Pickard, W. J. Emery, and J. H. Swift, 2011. *Descriptive Physical Oceanography: An Introduction*. 6th ed. Elsevier, 560 pp.
- Tomczak, M., and S. Liefink, 2005: Interannual variations of water mass volumes in the Southern Ocean. *J. Atmos. Ocean Sci.*, **10**, 31–42.
- Tomita, H., S. Kako, M. F. Cronin, and M. Kubota, 2010: Preconditioning of the wintertime mixed layer at the Kuroshio Extension Observatory. *J. Geophys. Res.*, **115**, C12053, doi:10.1029/2010JC006373.
- Uda, M., 1955: On the subtropical convergence and the currents in the Northwestern Pacific. *Rec. Oceanogr. Workshop Japan*, **2**, 141–150.
- , and K. Hasunuma, 1969: The eastward Subtropical Countercurrent in the western North Pacific Ocean. *J. Oceanogr. Soc. Japan*, **25**, 201–210.
- van der Werf, P. M., M. W. Schouten, P. J. V. Leeuwen, H. Ridderinkhof, and W. P. M. d. Ruijter, 2009: Observation and origin of an interannual salinity anomaly in the Mozambique Channel. *J. Geophys. Res.*, **114**, C03017, doi:10.1029/2008JC004911.
- van Sebille, E., M. O. Baringer, W. E. Johns, C. S. Meinen, L. M. Beal, M. F. de Jong, and H. M. van Aken, 2011: Propagation pathways of classical Labrador Sea water from its source region to 26°N. *J. Geophys. Res.*, **116**, C12027, doi:10.1029/2011JC007171.
- Williams, P. D., E. Guilyardi, R. Sutton, J. Gregory, and G. Madec, 2007: A new feedback on climate change from the hydrological cycle. *Geophys. Res. Lett.*, **34**, L08706, doi:10.1029/2007GL029275.
- Wyrski, K., 1975: Fluctuations of the dynamic topography in the Pacific Ocean. *J. Phys. Oceanogr.*, **5**, 450–459.
- Yan, Y., D. Xu, Y. Qi, and Z. Gan, 2012: Observations of freshening in the northwest Pacific subtropical gyre near Luzon Strait. *Atmos.–Ocean*, **50** (Suppl.), 92–102, doi:10.1080/07055900.2012.715078.
- Yeager, S. G., and W. G. Large, 2004: Late-winter generation of spiciness on subducted isopycnals. *J. Phys. Oceanogr.*, **34**, 1528–1547.